Environ Earth Sci (2012) 65:441–451
DOI 10.1007/s12665-011-1009-9

SPECIAL ISSUE

Arsenate adsorption at the sediment–water interface: sorption experiments and modelling

Laura Borgnino · Carlos P. De Pauli · Pedro J. Depetris

Received: 24 June 2010 / Accepted: 9 March 2011 / Published online: 24 March 2011

Abstract Arsenate adsorption was studied in three clastic sediments, as a function of solution pH (4.0–9.0) and arsenate concentration. Using known mineral values, protolytic constants obtained from the literature and K_{ads} values (obtained by fitting experimental adsorption data with empirical adsorption model), the constant capacitance surface complexation model was used to explain the adsorption behavior. The experimental and modelling approaches indicate that arsenate adsorption increases with increased pH, exhibiting a maximum adsorption value before decreasing at higher pH. Per unit mass, sample S_3 (smectite–quartz/muscovite–illite sample) adsorbs more arsenate in the pH range 5–8.5, with 98% of sites occupied at pH 6. S_1 and S_2 have less adsorption capacity with maxima adsorption in the pH ranges of 6–8.5 and 4–6, respectively. The calculation of saturation indices by PHREEQC at different pH reveals that the solution was undersaturated with respect to aluminum arsenate ($AlAsO_4 2H_2O$), scorodite ($FeAsO_4 2H_2O$), brucite and silica, and supersaturated with respect to gibbsite, kaolinite, illite and montmorillonite (for S_3 sample). Increased arsenate concentration (in isotherm experiments) may not produce new solid phases, such as $AlAsO_4 2H_2O$ and/or $FeAsO_4 2H_2O$.

L. Borgnino · P. J. Depetris
CICTERRA, Universidad Nacional de Córdoba,
Ciudad Universitaria, 5000 Córdoba, Argentina
e-mail: pdepetris@efn.uncor.edu

L. Borgnino (✉) · C. P. De Pauli
INFIQC, Universidad Nacional de Córdoba,
Ciudad Universitaria, 5000 Córdoba, Argentina
e-mail: borgnino@fcq.unc.edu.ar

C. P. De Pauli
e-mail: depauli@fcq.unc.edu.ar

Keywords Sediment–water interface · Adsorption · Surface complexation model · Arsenate · Clays

Introduction

Aquifers used to supply drinking water in many countries worldwide continue to be enriched with As, causing serious health problems related to its known toxicity (Kapaj et al. 2006; Hopenhayn 2006; Singh et al. 2007). The presence of As in soils, sediments and water is attributed to natural sources, such as the weathering of minerals with high As contents, and to human activities (use of arsenical fertilizers, pesticides, industrial and mining activities) (Smedley and Kinniburgh 2002). Although anthropogenic sources have contributed to the increase of As concentration in groundwater, in global terms the natural weathering of As-bearing rocks (Guillot and Charlet 2007) is the dominant mechanism of As enrichment in drinking water reservoirs, e.g., Bangladesh, India, Vietnam, Argentina, Chile, Mexico and Brazil (Smedley and Kinniburgh 2002).

The geochemical control of As retention in sediments is important to health risk assessments and remediation strategies, because its toxicity, mobility and bioavailability are functions of its state and local chemical environment (Beaulieu and Savage 2005). Furthermore, As dynamics in soils is largely controlled by the properties (including pH, redox potential and other ions competing for sorption sites) that influence its adsorption onto mineral and colloid surfaces, such as iron, aluminum and manganese (oxy)hydroxides, and clay minerals (Beaulieu and Savage 2005). In connection with this, previous research has shown that arsenate adsorption is related to Al and Fe (oxy)hydroxides, and to the clay content of sediments (Jiang et al. 2005). Therefore, its adsorption capacity

depends on both, the number of reactive hydroxyl sites and sediment surface area. Fe/Al (oxy)hydroxides, especially the less crystalline forms, adsorb more As per unit mass than several clay minerals (Goldberg 2002). However, the Fe/Al (oxy)hydroxide contents in sediments are lower than the clay mineral contents (Wisawapipat et al. 2009), so that the adsorption capacity of sediments must be mainly determined by the number of reactive surface groups that clay minerals expose. During the last few years, a relative large number of studies were performed investigating the arsenate adsorption onto clay minerals such as montmorillonite, kaolinite and illite (Manning and Goldberg 1996; Goldberg 2002). Fewer were made using whole sediments or soils (Jiang et al. 2005; Goldberg et al. 2005), or one of its grain-size mineral fractions.

Surface complexation models (SCM) have been widely used to describe the anion adsorption on single mineral and sediment water interface (Kooner et al. 1995; Manning and Goldberg 1996; Goldberg 2002; Goldberg et al. 2005; Chakraborty et al. 2007; Missana et al. 2009). SCM describe adsorption in terms of chemical reactions between surface functional groups and the total dissolved chemical species in the liquid media. The models most commonly used to describe the solid–liquid interface are the constant capacitance model, CCM (Schindler and Gamsjäger 1972), the diffuse layer model, DLM (Stumm et al. 1970), and the three layer models, TLM (Davis et al. 1978). Each model assumes a particular interfacial structure, resulting in the consideration of a surface reaction. The typical 2-pK model contains a reactive surface group, SOH, which undergoes both protonation and dissociation reactions, while the 1-pK model (Borkovec 1997) just uses a single equilibrium. Other recent models are the multisite complexation (MUSIC) (Hiemstra et al. 1989a, b) and the charge distribution CD-MUSIC models (Hiemstra and van Riemsdijk 1996).

The CCM has been applied to describe adsorption on single mineral phases and soils. Ions that have been studied include phosphate (Goldberg and Sposito 1984), borate (Goldberg et al. 2000, 2004), selenite (Goldberg and Glaubig 1988), arsenate (Manning and Goldberg 1996; Goldberg 2002) and molybdate (Goldberg 2002). These studies usually consider that a generic surface functional group represents the average surface properties of the soil or sediment. This is the generalized composite (GC) approach (Goldberg et al. 2007). Besides, in most of these reports the protolytic constant used was the average values of aluminum and iron oxide minerals obtained from literature and the K_{ads} values that are the result of fitting processes.

The aim of the present study was to understand the role of the silt-sized sediment (< 63 μm) fraction in arsenate adsorption, using experimental approach and surface complexation modelling. Mineralogical, chemical and surface characterizations are investigated to identify individual component minerals that control the surface reactivity of sediment particles. The dependence of pH and of different initial arsenate concentrations on adsorption behavior was evaluated. For the modelling exercise, known values of mineral protolytic constants (illite, montmorillonite) obtained from literature and K_{ads} values (obtained by fitting experimental adsorption data with empirical adsorption model) were used as initial parameters in the modelling fitting procedure. To understand if change in pH or increased arsenate initial concentration might have influence on sediments dissolution, the release of different elements during adsorption experiments was also studied. The obtained results may contribute to understand the mobility and bioavailability of arsenate in contaminated aquifers and groundwater resources.

Materials and methods

Characterization of the silt-sized fraction

Three samples of clastic sediments (S_1, S_2 and S_3) were collected from the Eureka mine (Córdoba, Argentina). After sieving, a portion of the silt-sized fraction (<63 μm) was separated and stored for chemical and mineralogical analyses. The mineralogy of the <63 μm and their <2 μm fractions was determined by X-ray diffraction (XRD) analysis, performed on a Philips X′Pert PRO X-ray diffractometer operating at 30 kV and 15 mA and using Cu–Kα radiation. Measurements were performed on both random (<63 μm) and oriented (<2 μm clay fraction) samples. Oriented slides were tested in air-dried, ethylene glycolated and 550°C calcinated preparations. XRD data were obtained in the 2θ range from 4 to 70° (step size: 0.02; 3.5 seg/step) for random samples and from 2 to 30° (0.03/2 s) for oriented samples. The reflection assignments were done using the software X′Pert HighScore, installed on the X-ray diffractometer.

The chemical analyses of sediments were performed by ICP/OES after a lithium metaborate/tetraborate fusion.

The specific surface area (SSA) was measured by the single-point N_2 adsorption method with a STROHLEIN area meter II instrument. An appropriate amount of dry solid (previously outgassed at 105°C) was placed in contact with N_2 and the system was cooled to 77 K to produce and quantify the gas adsorption. The SSA of the sample was calculated from the adsorbed amount, taking into account that each N_2 molecule covers an area of 16°$Å^2$.

The electrophoretic mobilities (EM) measurements were carried out using a Delsanano Size (Beckman) apparatus. Approximately, 200 mL of a dilute suspension (0.02 g

approximately) was prepared by dispersing the samples in 0.01 M $NaNO_3$. The suspension pH was raised to approximately nine with NaOH and the EM measurement was carried out. After that, the pH was slightly decreased with HCl and a new measurement performed. This procedure was continued until the pH was around 3.5.

Adsorption experiments

Arsenate adsorption kinetics experiments were carried out in 50-ml polyethylene centrifuges tubes, precleaned with 1% HNO_3 and rinsed several times with MilliQ water. Known amounts of each sample were suspended in 0.01 M $NaNO_3$. After 24 h of pre-equilibration, a well-known volume of a 0.01 M arsenate solution ($Na_2HAsO_4.7H_2O$) prepared in 0.01 M $NaNO_3$ was added and the pH of the suspension was adjusted by the addition of HNO_3 or NaOH until pH 5.5. This time was set as the initial time of the kinetics adsorption experiment. At different reaction times, an aliquot was withdrawn, centrifuged at 9,000 rpm during 10 min and filtered through a 0.45-μm cellulose membrane filter. The filtrate was stored at 4°C, after acidification with HNO_3 until analyzed by ICP-OES for total As.

Adsorption edges and isotherms were carried out in the same way as kinetics was performed. The pH value elected for isotherm experiments (5.0 for S_2 and 6.0 for S_1 and S_3 samples) is related to the maximum pH range for arsenate adsorbed, obtained in edge isotherm. The experimental conditions for edges and isotherms are listed in Table 1 and the equilibration times were set according to the kinetics experimental results. Once the equilibration time was reached, an aliquot was withdrawn, centrifuged and the filtrate was acidified and stored at 4°C to determine the As, Si, Al, K and Fe contents. The detection limits was 30 μg L^{-1} for As, 0.1 mgL^{-1} for Al, K and Si, and 0.01 mgL^{-1} for Fe.

Isotherm equations

As will be discussed below, the arsenate adsorption on S_1 and S_3 is indicative of the presence of at least two types of surface hydroxyl group. This approach was previously proposed (Sposito 1984; Bolt and Van Riemsdijk 1987; Bradbury and Baeyens 2002; Bradbury and Baeyens 2009; Chakraborty et al. 2007) and used in this work to investigate arsenate adsorption. In these cases, Freundlich equation is suitable to fit arsenate isotherms (Eq. 1). It is worth mentioning that the Freundlich model is empirical in nature and indicative of the surface heterogeneity of the adsorbent. It can be conceptualized as the sum of individual Langmuir isotherms, with a log-normal distribution of their affinity constants (Sposito 1984; Kinniburgh et al. 1983; Hinz et al. 1994). Based on this concept, we used first the linear form of Freundlich equation to fit arsenate isotherms and then Langmuir equation (Eq. 2) to obtain the corresponding adsorption constants ($K\text{ads}_{st}$ and $K\text{ads}_{wk}$) and the Γ_{max} for each surface site.

$$\Gamma = K_f C^n \quad (1)$$

where K_f (L g^{-1}) and n are constant

$$\Gamma = \frac{\Gamma_{max} K_{ads} C}{(1 + K_{ads} C)} \quad (2)$$

where K_{ads} is the constant related to the energy of adsorption (μmol L^{-1}) and Γ_{max} (μmol g^{-1}) is the adsorption maximum.

Modelling

The arsenate sorption dependence on pH was modelled considering protonation–deprotonation edges reactions, and inner-sphere complexation of the arsenate species. The K_{ads} and Γ_{max} obtained in the Langmuir isotherm fitted data were used as initial parameters in the modelling fitting procedure. Besides, just like with phosphate (Borgnino et al. 2010a), arsenate might not enter the phyllosilicate interlayer and only surface sites located in phyllosilicate edges were able to sorbs arsenate. The CCM was applied to describe the charge distribution and the potential decay on the aqueous side of the edge interface. This approach was previously used in studies dealing with oxides and clays minerals (Du et al. 1997a, 1997b; Goldberg 2002; Chakraborty et al. 2007; Gu and Evans 2007; Missana et al. 2009).

Table 1 Experimental conditions used in adsorption edges and isotherm experiments

	Adsorption edge			Adsorption isotherm		
	S_1	S_2	S_3	S_1	S_2	S_3
pH	4.1–9.2	4.1–9.1	4.1–9.1	6.0 ± 0.2	5.0 ± 0.2	6.0 ± 0.2
$[As]_0$ (μM)	15 ± 1.0	15 ± 1.0	15 ± 1.0	0.5–290	0.5–290	0.5–680
Suspension density (g L^{-1})	4.0 ± 0.2	4.0 ± 0.2	4.0 ± 0.2	4.0 ± 0.2	4.0 ± 0.2	4.0 ± 0.2

Ionic strength: 0.01 M $NaNO_3$, Equilibration time: 124 h

The following choices were taken in the model of our adsorption data:

(a) The surface hydroxyl group (edge groups) forms ionized surface sites at the protonation and dissociation reactions. We consider these binding sites as the one responsible for all surface complexation reactions with arsenate ions. The surface site is described by two protonation reactions with K_1 (Eq. 3) and K_2 (Eq. 4) as equilibrium protolytic constants:

$$SOH_2^+ \leftrightarrows SOH + H^+ \quad K_1 \tag{3}$$

$$SOH \leftrightarrows SO^- + H^+ \quad K_2 \tag{4}$$

where SO^-, SOH and $SOH_2{}^+$ are deprotonated, monoprotonated and diprotonated groups, respectively.

(b) The arsenate ions were considered to form inner-sphere surface complexes and only monodentate species were chosen. Reactions are written starting with the completely undissociated acids. Therefore, the surface complex reactions for arsenate are as follows

$$SOH + H_3AsO_4 \leftrightarrows S - H_2AsO_4 + H_2O \quad K_{1ads} \tag{5}$$

$$SOH + H_3AsO_4 \leftrightarrows S - HAsO_4^- + H_2O + H^+ \quad K_{2ads} \tag{6}$$

$$SOH + H_3AsO_4 \leftrightarrows S - AsO_4^{2-} + H_2O + 2H^+ \quad K_{3ads} \tag{7}$$

All our experimental data were obtained for a system with ionic strength 0.01 M $NaNO_3$, which remained constant during the adsorption process. Thus, all calculated equilibrium constants are conditional and valid only for this ionic strength. The optimizations of the equilibrium constant and the surface speciation of arsenate species were evaluated using the hydrogeochemical code PHREEQC 2.16 (Parkhust and Appelo 1999) using the Wateq4f database. Some parameters are required before surface complexation modelling can be applied to experimental adsorption data: (a) the number of binding sites (mol of sites), (b) the specific surface area of sorbent material ($m^2\ g^{-1}$) and (c) the mass of reactive material ($g\ L^{-1}$)

Results and discussion

Mineralogical, chemical and surface characterization

The XRD patterns of the three random samples are shown in Fig. 1. The pattern of S_1 and S_2 are typical of illite, muscovite and quartz, whereas some smectite/illite, quartz and feldspar seem to be present in the S_3 sample (Moore and Reynolds 1989). A better identification of the major, minor and accessory minerals was obtained with the XRD pattern on oriented samples. The results, for the respective minerals, were the following, respectively:

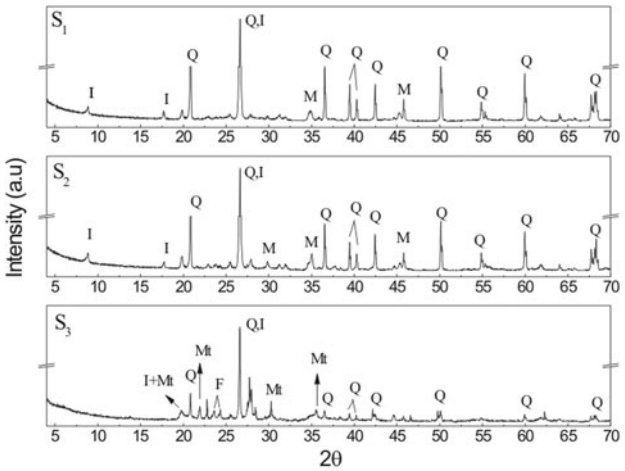

Fig. 1 XRD patterns of the three random samples. *Q* quartz, *I* illite, *M* muscovite, *Mt* montmorillonite, *F* feldspars

S_1: illite/muscovite–quartz
S_2: quartz/muscovite–illite/plagioclase
S_3: smectite–quartz–plagioclase/muscovite–illite–feldspar/anfibol

The bulk chemical composition of the samples is presented in Table 2, as well as the specific surface area. The chemical composition is rather similar for the three samples. High content of Si and Al indicate the presence of aluminosilicates and quartz as main minerals, which is in agreement with XRD results. In addition, a significant content of Fe, Na, Ca and Mg is also present in S_3, and K in S_1 and S_2. This seems to be related to the presence of smectite in S_3 sample and muscovite/illite in S_1 and S_2. The specific surface area of the samples ranges between 5.3 and 35.8 $m^2\ g^{-1}$, values that are in agreement with typical SSA obtained with the N_2 method for phyllosilicate minerals such as illite, smectites and kaolinite (Manning and Goldberg 1996; Goldberg 2002; Chakraborty et al. 2007).

Figure 2 shows the EM versus pH curves of the three studied samples in 0.01 M $NaNO_3$ solutions. All samples show a very similar behavior, with EM always negative and almost unchanged between pH 3 and 9. According to data obtained from chemical and mineralogical composition, quartz and phyllosilicates (illite and smectites) dominate the mineral composition and their presence is

Table 2 Chemical composition and SSA of studied samples

Sample	SSA ($m^2\ g^{-1}$)	Chemical composition (%)						
		SiO_2	Al_2O_3	Fe_2O_3	Na_2O	CaO	K_2O	MgO
S_1	5.3	82.23	10.05	0.52	0.07	0.15	2.91	0.2
S_2	10.5	76.1	13.62	1.33	0.41	0.28	3.92	0.33
S_3	35.8	57.27	16.74	5.28	2.44	2.21	1.72	1.73

reflected on the EM measurements, since they are always negatively charged in the whole studied pH range. This is an expected behavior since mica, clay minerals and quartz are typical acidic PZC minerals (Stumm 1992; Mukhopadhyay and Walther 2001; Taubaso et al. 2004; Jara et al. 2005; Borgnino et al. 2010b). Moreover, the presence of clay minerals that carry a net negative charge may contribute to the curve flatness of the electrophoretic mobilities versus pH curves, as shown in Fig. 2.

Adsorption kinetics

Figure 3 shows the adsorption kinetics for each sample at pH 5.5 and initial As concentration of 15 μM. All curves have similar characteristics, showing an important and fast adsorption between $t = 0$ and 10 h, and a slower adsorption at longer times. Adsorption seemed to reach completion at around 140 h (6 days), so this time was elected as equilibration time for edge and isotherm adsorption experiments. It is worth mentioning that this equilibrium time is much longer in relation to another described for As adsorption on minerals surfaces (i.e., Fe hydr(oxides). For instance, As adsorption on goethite seems to reach completion at around 5 h (Luengo et al. 2006), 6 h on Fe-coated zeolite (Jeon et al. 2009) or 24 h onto granular ferric hydroxide (Banerjee et al. 2008). Moreover, Manning and Goldberg (1996); Goldberg et al. (2002) found that 20 h was the time necessary to achieve equilibrium for arsenate adsorption on illite, montmorillonite and kaolinite samples. However, slow processes (i.e., diffusion controlled reactions on external and internal surface sites) usually control the adsorption kinetics in sediments (Sparks 1995). Certainly, an important factor controlling cation exchange reactions onto clay minerals is its multilayer staking structure. Mica, smectite and vermiculite, in which the permanent charge resides in part in the tetrahedral sheet, could generate a strong attractive interaction between the interlayer cations and the clay layer, leading to the formation of platelets, which could then have a further arrangement as aggregates (Avena 2002). Accordingly, the longer times observed for As adsorption in S_1, S_2 and S_3 sediment samples may be a consequence of clay aggregation, which reduces the accessibility of the surface sites or at least retards the diffusion kinetics. Chakraborty et al. (2007) found similar results for a muscovite and biotite mica.

Adsorption isotherm and edges

The adsorption isotherm and pH adsorption edge for arsenate on S_1 are shown in Fig. 4. When data are fitted using Freundlich isotherm, a good fit can be obtained (inset Fig. 4a) with log $Kf = 4.01$, $n = 0.83$ and $R^2 = 0.97$ ($p < 0.001$). This result indicates that at least two sorption sites are present, one with a strong affinity but scarce (6.0 ± 0.6 μmol g^{-1}), and the other with a weak affinity but more abundant (30 ± 0.8 μmol g^{-1}). The values of K_{ads} and Γ_{max} for each site, obtained from Langmuir isotherm, were used as starting fitting values to model pH adsorption edge. Furthermore, we used known parameters of Na-illite protolytic constants (Avena and De Pauli 1998), since this phyllosilicate predominates in the mineral composition of the sample. In this way, the only adjusted parameters were K_{ads} values.

Figure 4b shows the pH arsenate adsorption dependency. The dotted line corresponds to the best fit of experimental data, and the parameters used are given in

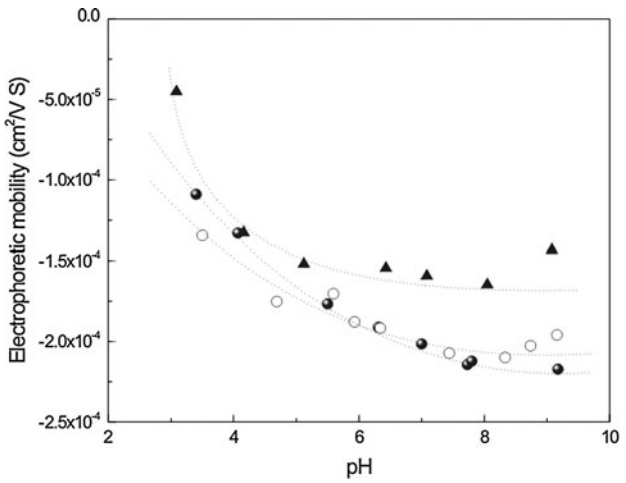

Fig. 2 Electrophoretic mobilities for S_1, S_2 and S_3 samples in 0.01 M $NaNO_3$

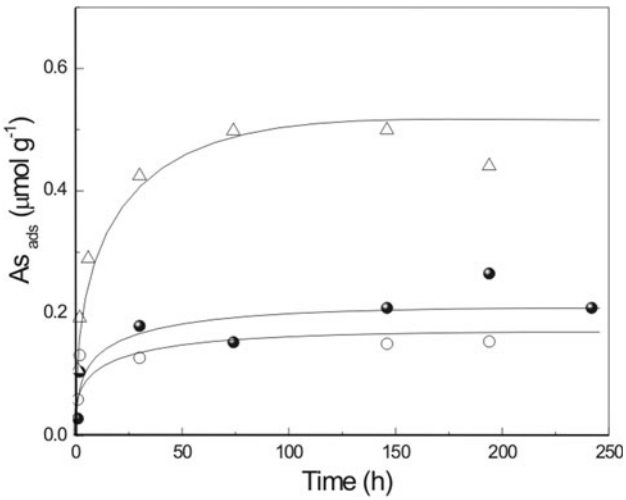

Fig. 3 As adsorption kinetics: $[As]_o = 15$ μM; pH: 5.5; suspension density: 4.0 g L^{-1}. *Solid circles* S_1 sample, *open circle* S_2 sample, *triangles* S_3 sample. *Lines* are drawn only to serve as guides to the eyes

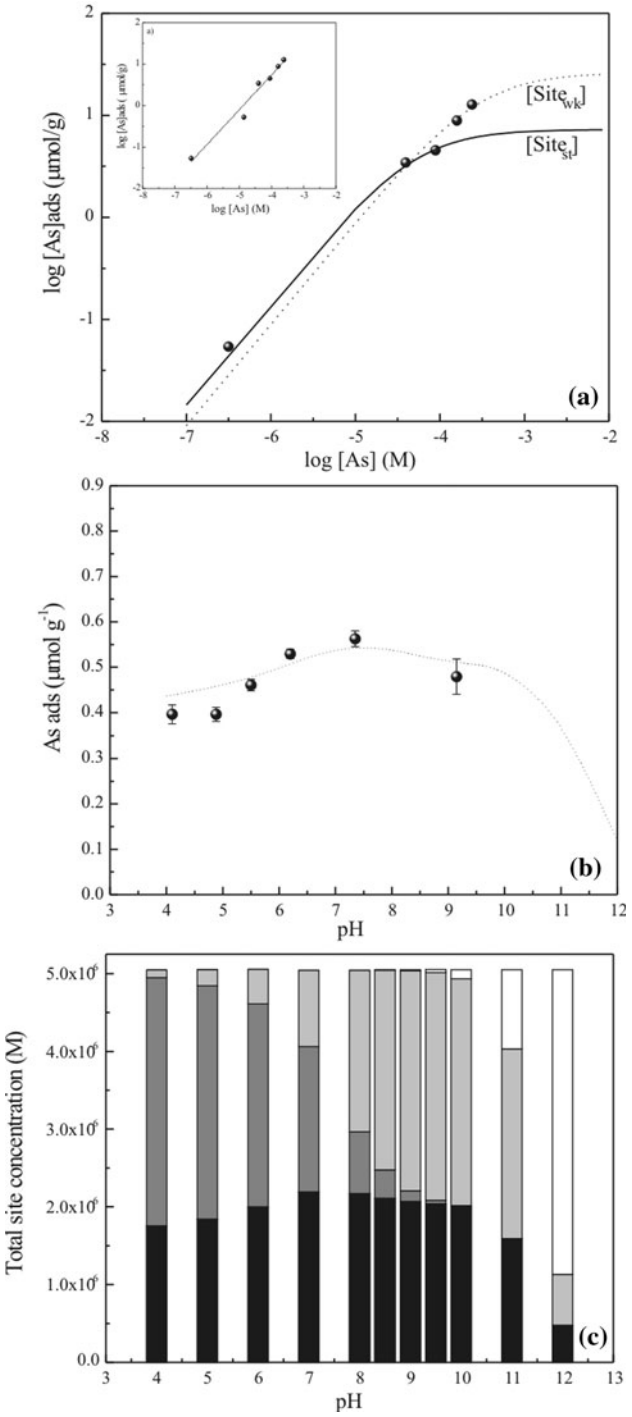

Fig. 4 Arsenate adsorption onto S_1. **a** Adsorption isotherm at pH ~6 and Langmuir fit to each surface site. Inset: Freundlich fit to the isotherm data with log K$f = 4.01$, $n = 0.83$, $R^2 = 0.97$. **b** Sorption pH dependence. *Lines* were fitted with PHREEQC, according to the model proposed. **c** Total surface speciation. *Black box* total (strong + weak) S-AsO_4^{2-} site, *dark gray box* SOH_2^+ site, *weak gray box* SOH site, *white box* SO^- site. The concentrations were obtained from the model predictions calculated with parameters in Table 3

Table 3. For this sample, the K_{ads} values obtained from the Langmuir isotherm hardly had to be adapted to achieve a satisfactory fit. The arsenate sorption onto S_1 had a maximum in the pH range 5.5–8.5, with a maximum at pH 7. The adsorption decreased from pH 8 toward alkaline pH values and under more acidic conditions (pH < 5.5). As will be discussed ahead, this is most likely due to an increased illite dissolution along the edges toward low pH. Similar results were obtained for arsenate adsorption onto illite, montmorillonite and kaolinite (Manning and Goldberg 1996; Goldberg et al. 2002) and onto muscovite and biotite mica (Chakraborty et al. 2007). The maximum pH value is almost coincident with the PZNPC value known for a Na-illite in 0.01 M $NaNO_3$ (Avena and De Pauli 1998), indicating that when the net proton edge charge is zero ($\sigma_H = 0$) the electrostatic repulsion between net negative surface charge and arsenate ions decreases and higher adsorption takes place. The surface speciation (Fig. 4c) indicates that the S_{st}-AsO_4^{2-} and S_{wk}-AsO_4^{2-} species (black box in Fig. 4c) are dominated in all the pH range, and both sites (S_{wk} and S_{st}) are needed to reproduce the sorption isotherm. As pH decreases from 7 to 4, the concentration of SOH_2^+ sites (dark gray boxes) increases in relation to S_{wk}-AsO_4^{2-} and S_{st}-AsO_4^{2} sites, indicating that the surface is more reactive to proton than arsenate ions. This phenomenon together with some illite edge dissolution may explain the slight decrease of adsorption at low pH. At pH 7 to 10, the adsorption is almost the same, and while pH rises the increase of SO^- sites (white box) increase the electrostatic repulsion between the charged surface and arsenate ions and make adsorption difficult.

Arsenate adsorption onto S_2 sample is represented in Fig. 5a, b. In contrast to sample S_1, only one site was necessary to achieve a good fit of experimental data. The maximum sorption level and K_{ads} values obtained through Langmuir fit are listed in Table 3 and, in this case, those values did not have to be adapted to reach a satisfactory fit. The acid–base log K values indicate a PZC of 2.95, a value observed for quartz mineral (Xu and Axe 2005; Kosmulski 2009). This is in agreement with our mineralogical data, inasmuch as quartz dominates in the sample. The pH sorption dependency is rather different form S_1 sample. Adsorption of arsenate shows a maximum in the pH range 4–6, decreases steeply toward alkaline pH and is dominated by S-AsO_4^{2-} surface species (Fig. 5c). The affinity of the surface toward protons and arsenate ions is very similar at pH 5 (Fig. 5c), achieving at such pH the maximum adsorption capacity of the sample. At higher pH, the SO^- site concentration increases, the electrostatic repulsion also increases and arsenate adsorption decreases.

Table 3 Arsenate adsorption onto S_1, S_2 and S_3 samples' model parameters obtained from the fits shown in Figs. 4, 5 and 6

Langmuir isotherm	Site concentration (μmol g^{-1})		
	S_1	S_2	S_3
$Site_{(wk)}$	30.0 ± 0.8	43.0 ± 0.2	18.0 ± 0.4
$Site_{(st)}$	6.0 ± 0.6	–	2.5 ± 0.1
Model reactions	Log K_{ads}		
	S_1	S_2	S_3
$S_{(st)}OH + H^+ \leftrightarrows S_{(st)}OH_2^+$	3.9	2.9	2.97
$S_{(st)}OH \leftrightarrows S_{(st)}O^- + H^+$	−7.6	−3.0	−6.1
$S_{(wk)}OH + H^+ \leftrightarrows S_{(wk)}OH_2^+$	3.9	2.9	2.9
$S_{(wk)}OH \leftrightarrows S_{(wk)}O^- + H^+$	−7.6	−3.0	−3.0
$S_{(st)}OH + H_3AsO_4 \leftrightarrows S_{(st)}\text{-}H_2AsO_4 + H_2O$	4.4 ± 0.2	–	4.5 ± 0.1
$S_{(st)}OH + H_3AsO_4 \leftrightarrows S_{(st)}\text{-}HAsO_4^- + H_2O + H^+$	4.4 ± 0.2	–	4.5 ± 0.1
$S_{(st)}OH + H_3AsO_4 \leftrightarrows S_{(st)}\text{-}AsO_4^{2-} + H_2O + 2H^+$	4.4 ± 0.2	–	4.5 ± 0.1
$S_{(wk)}OH + H_3AsO_4 \leftrightarrows S_{(wk)}\text{-}H_2AsO_4 + H_2O$	3.3 ± 0.5	3.0 ± 0.1	3.3 ± 0.5
$S_{(wk)}OH + H_3AsO_4 \leftrightarrows S_{(wk)}\text{-}HAsO_4^- + H_2O + H^+$	3.3 ± 0.5	3.0 ± 0.1	3.3 ± 0.5
$S_{(wk)}OH + H_3AsO_4 \leftrightarrows S_{(wk)}\text{-}AsO_4^{2-} + H_2O + 2H^+$	3.3 ± 0.5	3.0 ± 0.1	3.3 ± 0.5
Capacitance: 1.06 F m^{-2}			

The adsorption isotherm and pH dependence for S_3 sample are shown in Fig. 6a, b. Arsenate adsorption shows a maximum in the pH range 5–8.5, decreases toward acidic pH and more sharply toward alkaline pH (solid circles in Fig. 6b). A similar result was previously reported for montmorillonite (Manning and Goldberg 1996). As was indentified by XRD pattern, quartz and smectite predominate in the S_3 sample. Therefore to fit experimental data, a model represented by only the smectite site or quartz site (one-site model) was used as a first approach (continuous line in Fig. 6b). For the smectite site, known parameters of Na-montmorillonite protolytic constants (Avena and De Pauli 1998) with SSA of 25 m^2 g^{-1} (Tertre et al. 2006) were used. For quartz site, acid–base log K and SSA values assigned for S_2 sample were used and, in both cases, the total sites concentration and K_{ads} values was obtained thought Langmuir fit (total sites: 20.5 ± 0.8 μmol g^{-1}, log K_{ads}: 3.3 ± +0.2). Figure 6b shows the simulations obtained for arsenate adsorption onto these two single minerals. Despite the fact that the one-site model does not reproduce the sorption edge isotherm, it is useful for comparison purpose and to analyze the contribution of each mineral phase to the total surface adsorption properties of the sediment sample. The S_3 sample seems to be a mixture between these two minerals with a maximum adsorption value (per unit mass) as montmorillonite, but a maximum pH adsorption as quartz. Attempting to improve our model, we considered the existence of two sites (Fig. 6a), but in this case each site was discriminated between the weak and strong site such as quartz and montmorillonite sites, respectively. Using the same procedure as that applied in the S_1 sample, data were first fitted using Freundlich isotherm (inset Fig. 6a) and then with Langmuir isotherm for each site. The K_{ads} value and Γ_{max} obtained (Table 3) were used as starting fitting values to model the pH edge isotherm. The simulation is plotted as dotted lines in Fig. 6b. As seen in this figure, the two-site model broadly improved the goodness of fit, indicating that surface sites related to both minerals are necessary to reproduce the experimental data. Regarding the surface speciation, the $S_{wk}\text{-}AsO_4^{2-}$ and $S_{st}\text{-}AsO_4^{2}$ sites predominate in all the studied pH range, and at pH 6 almost all the sites (98%) are occupied by arsenate ions. As in the S_1 sample, some mineral dissolution and greater surface reactivity toward protons (pH <5), as well as higher electrostatic repulsion (pH >8.5), may explain the arsenate adsorption decrease in this pH range.

Release of different elements during arsenate adsorption

The concentration of Al, Si, Mg, Fe and K obtained from edge isotherms were plotted against pH (Fig. 7). The soluble content of K, Si and Mg were higher than that of Al and Fe, and in general the release increased with increasing pH under acidic conditions, minimizing at near neutral pH and increasing with increasing pH at alkaline conditions. Previous reports on dissolution rates found similar results (Huertas et al. 1999; Cama et al. 2000; Köhler et al. 2005; Rozalén et al. 2008). On the other hand, Kalinowski and Schweda (1996) reported dissolution rates of muscovite at

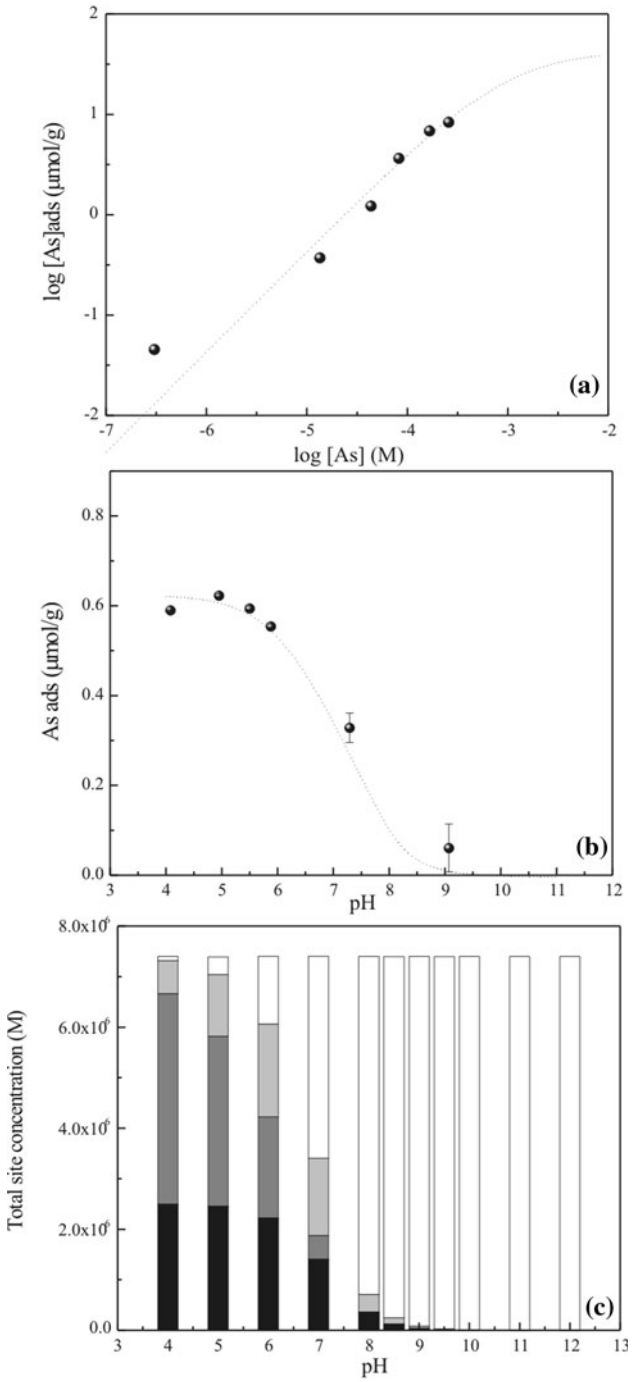

Fig. 5 Arsenate adsorption onto S_2. **a** Adsorption isotherm at pH ~5 and Langmuir fit to experimental data. **b** Sorption pH dependence. *Lines* were fitted with PHREEQC, according to the model proposed. **c** Total surface speciation. *Black box* S-AsO_4^{2-} site, *dark gray box* SOH_2^+ site, *weak gray box* SOH site, *white box* SO^- site. The concentration were obtained from the model predictions calculated with parameters in Table 3

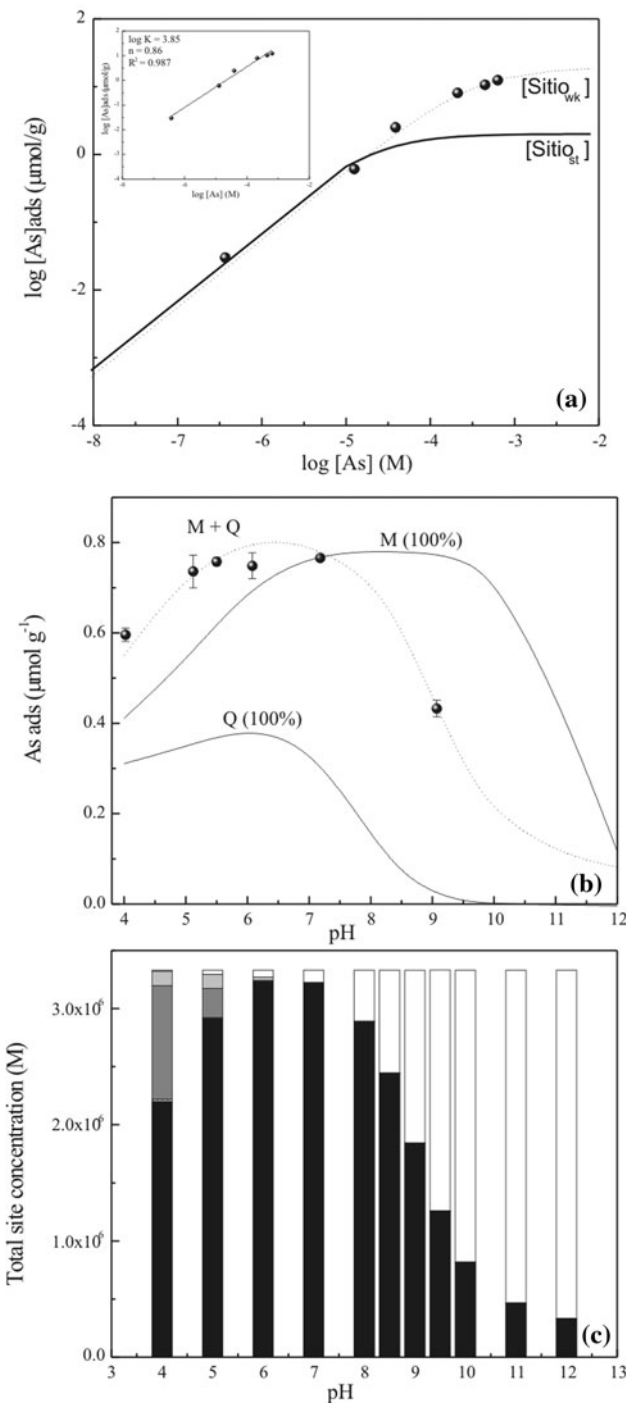

Fig. 6 Arsenate adsorption onto S_3. **a** Adsorption isotherm and Langmuir fit to each surface site at pH ~6. Inset: Freundlich fit to the isotherm data with log $Kf = 3.85$, $n = 0.86$, $R^2 = 0.987$. **b** Sorption pH dependence. *Lines* were fitted with PHREEQC, according to the model proposed: one-site model (continuous line); two-site model (dotted line). **c** Total surface speciation. *Black box* total (strong + weak) AsO_4^{2-} site, *dark gray box* SOH_2^+ site, *weak gray box* SOH site, *white box* SO^- site. The concentrations were obtained from the model predictions calculated with parameters in Table 3

pH 1–4 and suggested a dissolution mechanism involving inward movement of the dissolution front from the crystal edges. Consequently, the reactive surface edge of clay

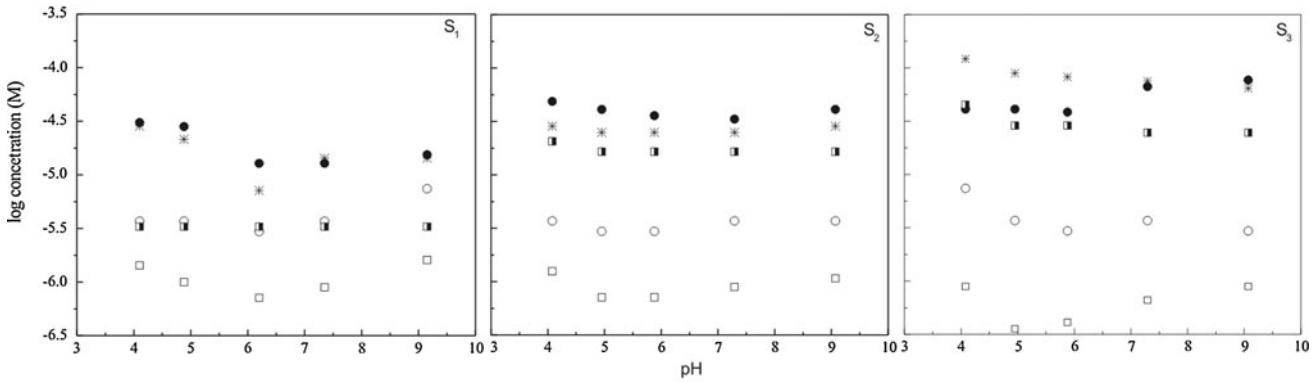

Fig. 7 Concentration of different elements during edge adsorption experiments. *Open circles* Al, *solid circles* K, *stars* Si, *square* Fe, solid *square* Mg

minerals and, therefore, the adsorption capacity may be affected by dissolution processes. Rozalén et al. (2008) also indicated that it was very difficult to achieve stoichiometry dissolution of aluminosilicates due to precipitation/sorption of Al (and Fe) secondary phases. For instance, gibbsite usually forms deposits on basal planes on 2:1 phyllosilicates from supersaturated solutions (Nagy et al. 1999); Fe released from the clay mineral framework precipitates as amorphous iron hydroxide. In contrast, Si is less likely to be incorporated into secondary phases. For the samples studied, the concentration of soluble Al, Fe and Si hardly changed with pH. Although the formation of secondary phases will probably occur, the large adsorption time necessary to achieve equilibrium (6 days) allows us to assume that some dissolution may occur at acidic pH. As a result, the decrease in arsenate adsorption at pH lower than 5 may be also a consequence of some clay dissolution along the edges.

The calculation of saturation indices was done by PHREEQC (Parkhust and Appelo 1999) using the Wateq4f database. The saturation indices show that our solutions were supersaturated with respect to gibbsite, kaolinite, illite and montmorillonite (for S_3 sample), and the Fe concentration was controlled by $Fe(OH)_3$ hydroxide precipitation. Furthermore, the solution was undersaturated with respect to aluminum arsenate ($AlAsO_4 2H_2O$), scorodite ($FeAsO_4 2H_2O$), brucite and silica. The saturation calculations also indicate that with increasing initial arsenate concentration, the solution approached, but did not reach, the solubility of $AlAsO_4 2H_2O$ and $FeAsO_4 2H_2O$. Therefore, increased arsenate concentration might have had no influence on clay mineral dissolution.

Conclusions

The constant capacity model was able to explain the arsenate adsorption onto the silt-size fraction of S_1, S_2 and S_3 sediment samples. Experimental and modelling indicated that the arsenate adsorption is pH dependent, increasing with increased pH, achieving a maximum adsorption value and then decreasing at higher pH. Per unit mass, S_3 adsorbs more arsenate in the 5–8.5 pH range, with 98% of the occupied sites at pH 6. Besides, in S_3 sample there were mixtures of single minerals, and the presence of quartz displaced the maximum pH adsorption value at lower pH, in relation to pure montmorillonite. S_1 and S_2 have less adsorption capacity (per unit mass) with a maximum adsorption value in the 5.5–8.5 and 4–6 pH range. Regarding clay mineral dissolution during adsorption experiments, increased initial arsenate concentration might have had no influence on dissolution and no secondary phases of arsenate ($AlAsO_4 2H_2O$ and $FeAsO_4 2H_2O$) were detected. Some edge clay dissolution at acidic pH also explains the decrease in arsenate adsorption at pH lower than 5. Arsenate retention on silt-size sediment fractions, in the 6–8 pH range (groundwater pH region), is higher than previous values reported for illite, montmorillonite (Goldberg 2002) and soils (Goldberg et al. 2005), but lower than muscovite and biotite samples (Chakraborty et al. 2007).

The findings obtained in the present study are of significance in understanding the role of the mineralogy composition of the silt-sized sediment fraction in the dynamic of arsenate in contaminated aquifers and groundwater resources. First, this study has shown that arsenate adsorption depends on the sediment mineralogy and on the number of reactive surface groups that minerals expose in the sediment–water interface. Sediment samples with a majority composition only in quartz and/or illite have less capacity to retain arsenate. Consequently, more arsenate remains in water and in this form it is more bioavailable to the aquatic environment. As the sediment composition is increased in other minerals (i.e., smectite), the number of surface sites increases, the adsorption capacity of sediments enhances, and therefore the arsenate in water could be accumulated onto the solid phase.

Moreover, a greater capacity for adsorption of the studied samples occurs in the pH range of 4–8, so sediments in contact with acidic or slightly alkaline water can act as a sink for arsenate.

As a closing remark of this study, it is necessary to make it clear that further experiments are necessary to evaluate the effect of competitors, such as phosphate, fluoride, carbonate, as well as the effect of organic matter in the adsorption of arsenate, in order to have a complete understanding of the mobility of arsenate in aquatic environments.

Acknowledgments This work was financed by Argentina's FONCYT, SECYT-UNC and CONICET. L Borgnino, C. P. De Pauli and P. Depetris are members of CICyT in Argentina′s CONICET.

References

Avena MJ (2002) Acid–base behavior of clay surfaces in aqueous media. In: Hubbard A (ed) Encyclopedia of surface and colloid science. Marcel Dekker, New York, pp 37–63

Avena MJ, De Pauli CP (1998) Proton adsorption and electrokinetics of an Argentinean montmorillonite. J Colloid Interf Sci 202:195–204

Banerjee K, Amy GL, Prevost M, Nour S, Jekel M, Gallagher PM, Blumenschein CD (2008) Kinetic and thermodynamic aspects of adsorption of arsenic onto granular ferric hydroxide (GFH). Water Res 42:3371–3378

Beaulieu BT, Savage K (2005) Arsenate Adsorption Structures on Aluminum Oxide and Phyllosilicate Mineral Surfaces in Smelter-Impacted Soils. Environ Sci Technol 39:3571–3579

Bolt GH, Van Riemsdijk WH (1987) Surface Chemical process in soils. In: Stumm W (ed) Aquatic Surface Chemistry. Wiley, New York

Borgnino L, Giacomelli CE, Avena M, De Pauli CP (2010a) Phosphate adsorbed on Fe(III) modified montmorillonite: Surface complexation studied by ATR-FTIR spectroscopy. Colloids Surf Physicochem Eng Aspects 353:238–244

Borgnino L, Garcia MG, del Hidalgo MV, Avena M, De Pauli CP, Blesa MA, Depetris PJ (2010b) Modeling the acid–base surface properties of aquatic sediments. Aquat Geochem 16:279–291

Borkovec M (1997) Origin of 1-pK and 2-pK models for ionizable water–solid interfaces. Langmuir 13:2608–2613

Bradbury MH, Baeyens B (2002) Sorption of Eu on Na and Ca- montmorillonite: experimental investigation and modeling with cation exchange and surface complexation. Geochim Cosmochim Acta 66:2325–2334

Bradbury MH, Baeyens B (2009) Sorption modeling on illite. Part I: titration measurements and sorption of Ni, Co, Eu and Sn. Geochim Cosmochim Acta 73:990–1003

Cama J, Ganor J, Ayora C, Lasaga CA (2000) Smectite dissolution kinetics at 80°C and pH 8.8. Geochim et Cosmochim Acta 64:2701–2717

Chakraborty S, Wolthers M, Chatterjee D, Charlet L (2007) Adsorption of arsenite and arsenate onto muscovite and biotite mica. J Colloid Interf Sci 309:392–401

Davis JA, James RO, Lechie JO (1978) Surface ionization and complexation at the oxide/water interface: I. Computation of electrical double layer properties in simple electrolytes. J Colloid Interf Sci 63:480–499

Du Q, Sun Z, Forsling W, Tang H (1997a) Acid–base properties of aqueous illite surfaces. J Colloid Interf Sci 187:221–231

Du Q, Sun Z, Forsling W, Tang H (1997b) Adsorption of copper at aqueous illite surfaces. J Colloid Interf Sci 187:232–242

Goldberg S (2002) Competitive adsorption of arsenate and arsenite on oxides and clay minerals. Soil Sci Soc Am J 66:413–421

Goldberg S, Glaubig RA (1988) Anion sorption on a calcareous, montmorillonitic soil–selenium. Soil Sci Soc Am J 52:954–958

Goldberg S, Sposito G (1984) A chemical model of phosphate adsorption by soils: II. Noncalcareous soils. Soil Sci Soc Am J 48:779–783

Goldberg S, Lesch SM, Suarez DL (2000) Predicting boron adsorption by soils using soil chemical parameters in the constant capacitance model. Soil Sci Soc Am J 64:1356–1363

Goldberg S, Lesch SM, Suarez DL (2002) Predicting molybdenum adsorption by soils using soil chemical parameters in the constant capacitance model. Soil Sci Soc Am J 66:1836–1842

Goldberg S, Suarez DL, Basta NT, Lesch SM (2004) Predicting boron adsorption isotherms by Midwestern soils using the constant capacitance model. Soil Sci Soc Am J 68:795–801

Goldberg S, Lesch SM, Suarez DL, Basta NT (2005) Predicting arsenate adsorption by soils using chemical parameters in the constant capacitance model. Soil Sci Soc Am J 69:1389–1398

Goldberg S, Criscenti LJ, Turner DR, Davis J, Cantreli KJ (2007) Adsorption–desorption process in subsurface reactive transport modeling. Vadose Zone J 6:407–435

Gu X, Evans LJ (2007) Modelling the adsorption of Cd(II), Cu(II), Ni(II), Pb(II) and Zn(II) onto Fithian illite. J Colloid Interf 307:317–325

Guillot S, Charlet L (2007) Bengal arsenic, an archive of Himalaya orogeny and paleohydrology. J Environ Sci Health A Tox Hazard Subst Environ Eng 42:1785–1794

Hiemstra T, van Riemsdijk WH (1996) A surface structural approach to ion adsorption: the charge distribution (CD) model. J Colloid Interf Sci 179:488–508

Hiemstra T, van Riemsdijk WH, Bolt GH (1989a) Multisite proton adsorption modeling at the solid/solution interface of (hydr) oxides: a new approach: I. Model description an evaluation of intrinsic reaction constants. J Colloid Interf Sci 133:91–104

Hiemstra T, De Wit JCM, van Riemsdijk WH (1989b) Multisite proton adsorption modeling at the solid/solution interface of (hydr)oxides: a new approach: II. Application to various important (hydr)oxides. J Colloid Interf Sci 133:105–117

Hinz C, Gaston LA, Selim HM (1994) Effect of sorption isotherm type on predictions of solute mobility in soil. Water Resour Res 30:3013–3021

Hopenhayn C (2006) Arsenic in drinking water: impact on human health. Elements 2:103–107

Huertas FJ, Chou L, Wollast R (1999) Mechamism of kaolinite dissolution at room temperature and pressure. II: kinetic study. Geochim et Cosmochim Acta 63:3261–3275

Jara AA, Goldberg S, Mora ML (2005) Studies of the surface charge of amorphous aluminosilicates using surface complexation models. J Colloid Interf Sci 292:160–170

Jeon C-S, Baek K, Park J-K, Oh Y-K, Lee S-D (2009) Adsorption characteristics of As (V) on iron-coated zeolite. J Hazard Mater 163:804–808

Jiang W, Zhang S, Shan X-Q, Feng M, Zhu Y-G, Mc Laren RG (2005) Adsorption of arsenate on soils. Part 2: Modeling the relationship between adsorption capacity and soil physicochemical properties using 16 Chinese soils. Environ Pollut 138:285–289

Kalinowski BE, Schweda P (1996) Kinetic of muscovite, phlogopite and biotite dissolution and alteration at pH 1–4 room temperature. Geochim et Cosmochim Acta 60:367–385

Kapaj S, Peterson H, Liber K, Bhattacharya P (2006) Human health effects from chronic arsenic poisoning: a review. J Environ Sci Health A Tox Hazard Subst Environ Eng 41:2399–2428

Kinniburgh DG, Barker JA, Whitefield M (1983) A comparison of some simple adsorption isotherms for describing divalent cation adsorption by ferrihydrite. J Colloid Interf Sci 95:370–384

Köhler SJ, Bosbach D, Oelkers EH (2005) Do clay mineral dissolution rates reach steady state? Geochim et Cosmochim Acta 69:1997–2006

Kooner ZS, Jardine PM, Feldman S (1995) Competitive surface complexation reactions of sulfate and natural organic carbon on soil. J Environ Qual 24:656–662

Kosmulski M (2009) pH-dependent surface charging and points of zero charge. IV. Update and new approach. J Colloid Interface Sci 337:439–448

Luengo C, Brigante M, Antelo J, Avena M (2006) Kinetic of phosphate adsorption on goethite: comparing batch adsorption and ATR-IR measurements. J Colloid Interf Sci 300:511–518

Manning B, Goldberg S (1996) Modeling Arsenate competitive adsorption on Kaolinite, montmorillonite and Illite. Clays Clay Miner 44:609–623

Missana T, Alonso U, Garcia-Gutierrez M (2009) Experimental study and modelling of selenite sorption onto illite and smectite clays. J Colloid Interf Sci 334:132–138

Moore DM, Reynolds RC (1989) X-ray diffraction and the identification and analysis of clay minerals. Oxford University Press, New York, p 249

Mukhopadhyay B, Walther JV (2001) Acid–base chemistry of albite surfaces in aqueous solutions at standard temperature and pressure. Chem Geol 174:415–443

Nagy KL, Cygan RT, Hanchar JM, Sturchio NC (1999) Gibbsite growth kinetics on gibbsite, kaolinite, and muscovite substrates: atomic force microscopy evidences per epitaxy and assessment of reactive surface area. Geochim et Cosmochim Acta 63:2337–2351

Parkhust DL, Appelo CA (1999) Users guide to PHREEQC, U.S. geological survey

Rozalén ML, Huertas FJ, Brady PV, Cama J, García-Palma S, Linares J (2008) Experimental study of the effect of pH on the kinetics of montmorillonite dissolution at 25°C. Geochim et Cosmochim Acta 72:4224–4253

Schindler PW, Gamsjäger H (1972) Acid–base reactions of the TiO_2 (Anatase) water interface and the point of zero charge of TiO_2 suspensions. Kolloid ZZ Polym 250:759–763

Singh N, Kumar D, Sahu AP (2007) Arsenic in the environment: effects on human health and possible prevention. J Environ Biol 28:359–365

Smedley PL, Kinniburgh DG (2002) A review of the source, behaviour and distribution of arsenic in natural waters. Appl Geochem 17:517–568

Sparks DL (1995) Environmental soil and chemistry. Academic Press, London

Sposito G (1984) The surface chemistry of soils. Oxford University Press, New York

Stumm W (1992) Chemistry of the solid–water interface. Wiley, New York

Stumm W, Huang CP, Jenking SR (1970) Specific chemical interaction affecting the stability of dispersed systems. Croat Chem Acta 42:223–245

Taubaso C, Dos Santos Afonso M, Torres Sánchez RM (2004) Modelling soil surface charge density using mineral composition. Geoderma 121:123–133

Tertre E, Castet S, Berger G, Loubet M, Giffaut E (2006) Surface chemistry of kaolinite and Na-montmorillonite in aqueous electrolyte solutions at 25 and 60°C: experimental and modeling study. Geochim et Cosmochim Acta 70:4579–4599

Wisawapipat W, Kheoruenromne I, Suddhiprakarn A, Gilkes RJ (2009) Phosphate sorption and desorption by Thai upland soils. Geoderma 153:408–415

Xu Y, Axe L (2005) Synthesis and characterization of iron oxide-coated silica and its effect on metal adsorption. J Colloid Interf Sci 282:11–19